PHILOSOPHICAL TRANSACTIONS OF THE ROYAL SOCIETY A MATHEMATICAL, PHYSICAL & ENGINEERING SCIENCES

Atomistic Modelling of Diffusional Phase Transformations

A. Cerezo, J. M. Hyde, M. K. Miller, S. C. Petts, R. P. Setna and G. D. W. Smith

Phil. Trans. R. Soc. Lond. A 1992 **341**, 313-326
doi: 10.1098/rsta.1992.0104

Atomistic modelling of diffusional phase transformations

By A. Cerezo[1], J. M. Hyde[1], M. K. Miller[2], S. C. Petts[1]†, R. P. Setna[1] and G. D. W. Smith[1]

[1] *Department of Materials, University of Oxford, Parks Road, Oxford OX1 3PH, U.K.*
[2] *Metals and Ceramics Division, Oak Ridge National Laboratory, Oak Ridge, Tennessee 37831-6376, U.S.A.*

A simple Monte Carlo model has been used to simulate diffusional phase transformations occurring in binary alloys during thermal ageing. The results of the simulation are compared directly with atomic-scale chemical information obtained from position-sensitive atom probe microanalysis. A simple pair potential model is found to give a good match with the ageing behaviour of spindodally decomposing iron–chromium alloys. Initial results on the modelling of nucleation and growth are presented, and compared with phase separation of copper–cobalt alloys.

1. Introduction

Conventional theories of diffusional phase transformations are based on continuum models, an approach which appears reasonable given the number of atoms in even a modest amount of material. However, advances in microscopy and microanalysis have extended the study of phase decompositions to the earliest stages, when composition fluctuations are on the scale of only a few atomic spacings. The properties of many technological alloys depend on variations in chemical composition at the nanometre scale. Structures of this size cannot be adequately represented using continuum representations of the composition, and this leads to a breakdown of conventional models in predicting the kinetics of the reactions. Understanding the early stages of phase decomposition is not only important at a fundamental level, but also for predicting the long-term stability of engineering alloys and in the design of new materials. This paper describes an attempt to provide a statistical, atomistic model of the ageing of materials, through the use of a Monte Carlo simulation. The modelling work is being performed in conjunction with an experimental programme of atomic-scale studies of the early stages of phase transformations. It is therefore possible to make direct comparisons between the results of the atomistic simulation and the atomic-scale chemical measurements.

2. Atom probe microanalysis

The technique of atom probe microanalysis (Müller *et al.* 1968) provides the chemical analysis of materials at the highest possible spatial resolution. (For a general review of the technique and its applications see, for example, Miller & Smith (1989).) In this instrument a specimen in the form of a sharp needle point is held in an ultra-high vacuum chamber and subjected to a high positive potential. The

† Present address: 65 Ferndale Road, New Milton, Hants BH25 5EX, U.K.

Phil. Trans. R. Soc. Lond. A (1992) **341**, 313–326
Printed in Great Britain

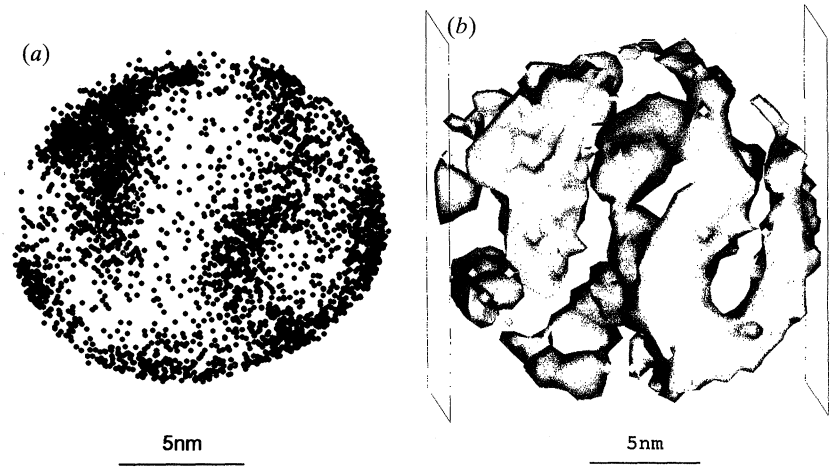

Figure 1. Position sensitive atom probe analysis of the ferrite phase in a CF3 duplex stainless steel (Fe, 21% Cr, 9% Ni, 0.4% Mn, 0.7% Si, 0.2% Mo, 0.02% C (all by mass)) aged for 10^4 hours at 400 °C. (*a*) Chromium atom map from a slice of material 2 nm deep, showing the clustering of chromium atoms into an interconnected structure during the thermal ageing. (*b*) Isosurface reconstruction of the microstructure from a region of material 15 nm in diameter and 10 nm deep. After a local sampling process, the surface is drawn through all points of composition 30 at.%, which represents the interface between chromium enriched and chromium depleted regions.

intense field is sufficient to ionize prominent atoms on the specimen surface, and the resulting ions travel along approximately radial paths away from the specimen point. This radial projection generates a magnification of approximately 10^6. A small aperture in the system selects ions from a region 1–2 nm in diameter on the specimen surface, allowing them to pass into a time-of-flight mass spectrometer. The elemental identification of single atoms removed from the surface gives a measurement of the local composition of the selected region, and continued removal gives a measurement of the variation of composition with depth, with single atomic layer depth resolution. A recent extension of this technique, the position sensitive atom probe (POSAP) (Cerezo *et al.* 1989) uses a position-sensitive detector to identify ions removed from a larger area (approximately 20 nm in diameter) on the specimen surface. From the position of arrival and identity of individual ions, an atomic map is built up of the distribution of elements on the specimen surface (figure 1*a*). Continued removal of material allows a full three-dimensional reconstruction of the atomic positions, and thus the variations in chemical composition (figure 1*b*). The POSAP analysis of the ferrite phase in a CF3 duplex stainless steel (Fe, 21% Cr, 9% Ni, 0.4% Mn, 0.7% Si, 0.2% Mo, 0.02% C (all by mass)), aged for 10^4 h at 400 °C is shown in figure 1. This example shows the analysis of a volume 15 nm in diameter and 10 nm in depth, showing the scale of the structures which are observable in the POSAP. Despite the significant thermal ageing of this material, the wavelength of the microstructure formed is less than 10 nm, or approximately 50 atom spacings.

3. Monte Carlo simulation

In the computer simulation, an alloy is represented by an Ising model with conserved order parameter. Atoms of type A or B (equivalent to spin-up or spin-down) are placed on a regular three-dimensional cubic lattice. Much of the simulation

PHILOSOPHICAL TRANSACTIONS OF THE ROYAL SOCIETY A MATHEMATICAL, PHYSICAL & ENGINEERING SCIENCES

has been done on a simple cubic lattice but body-centred and face-centred lattices have also been used. Diffusional processes in the solid are simulated either by atom swaps, or by a random walk of a vacancy through the lattice. At any stage, the new configuration (after an atom–atom or atom–vacancy swap) is accepted or discarded according to the change in energy $\Delta E = E_{i+1} - E_i$. The probability of acceptance is given by the Metropolis function (Metropolis *et al.* 1953):

$$W(X_i \to X_{i+1}) = \begin{cases} \exp(-\Delta E/kT) & \text{if} \quad \Delta E > 0, \\ 1 & \text{if} \quad \Delta E \leqslant 0. \end{cases}$$

To date, atomic binding has been represented in the model using a simple pair potential, and no atom–vacancy binding energy has been included. Although the modelling of diffusion by atom swaps is simpler, this method has the disadvantage that it can only model symmetrical systems, since the energy change on any swap will always be a multiple of the energy parameter

$$\alpha = E_{\mathrm{aa}} + E_{\mathrm{bb}} - 2E_{\mathrm{ab}},$$

where E_{aa} is the binding energy between two A atoms, E_{bb} is that between two B atoms, and E_{ab} the binding between two unlike atoms. There is no method by which a difference between E_{aa} and E_{bb} can be represented in the simulation. However, an atom–vacancy swap is described in terms of two energy parameters:

$$\alpha_1 = E_{\mathrm{aa}} - E_{\mathrm{ab}} \quad \text{and} \quad \alpha_2 = E_{\mathrm{bb}} - E_{\mathrm{ab}}.$$

To make a comparison between the two simulation methods, the binding energies for the two cases must be made identical, that is $\alpha_1 = \alpha_2 = \frac{1}{2}\alpha$. Under these conditions, no difference is found between simulations using atom swapping, and those which use vacancy diffusion (Yaldram & Binder 1991).

The regular solution model of an alloy is equivalent to a mean field approximation (MFA) for the binding of an atom in the solid, in which the enthalpy of a random mixture of N_{a} type A atoms and N_{b} type B atoms ($N = N_{\mathrm{a}} + N_{\mathrm{b}}$ total atoms) is given by

$$H = \frac{N_{\mathrm{a}}^2}{2N} mE_{\mathrm{aa}} + \frac{N_{\mathrm{b}}^2}{2N} mE_{\mathrm{bb}} + \frac{N_{\mathrm{a}} N_{\mathrm{b}}}{N} mE_{\mathrm{ab}} = \tfrac{1}{2}Nm\,[x^2 E_{\mathrm{bb}} + (1-x)^2 E_{\mathrm{aa}} + 2x(1-x)\,E_{\mathrm{ab}}],$$

where m is the coordination number and x is the atomic fraction of type B atoms. Including the entropy of the mixture

$$S = k \ln [N_{\mathrm{a}}!\,N_{\mathrm{b}}!/N!] \approx -kN[x \ln (x) + (1-x) \ln (1-x)]$$

gives the Gibbs free energy

$$G = N\{-\tfrac{1}{2}m[x^2(E_{\mathrm{aa}} + E_{\mathrm{bb}} - 2E_{\mathrm{ab}}) + 2x(E_{\mathrm{ab}} - E_{\mathrm{aa}}) + E_{\mathrm{aa}}] + kT[x \ln (x) + (1-x) \ln (1-x)]\}$$

or, for the symmetric case $E_{\mathrm{aa}} = E_{\mathrm{bb}}$,

$$G = N\{-\tfrac{1}{2}m[\alpha(x^2 - x) + E_{\mathrm{aa}}] + kT[x \ln (x) + (1-x) \ln (1-x)]\}.$$

The form of the Gibbs energy at low temperatures is shown in figure 2, showing two minima either side of a central maximum. It is the position of the minima that

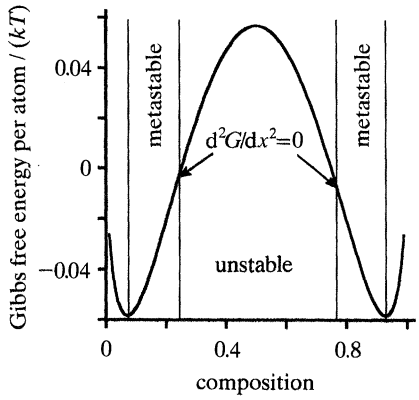

Figure 2. Gibbs free energy curve for a regular solid solution, under conditions where phase separation may occur. The region between the minima in the curve gives the miscibility gap. Within the $d^2G/dx^2 = 0$ points on the curve, the solution is unstable and can decompose through a spinodal reaction. Outside these points, the solution is metastable.

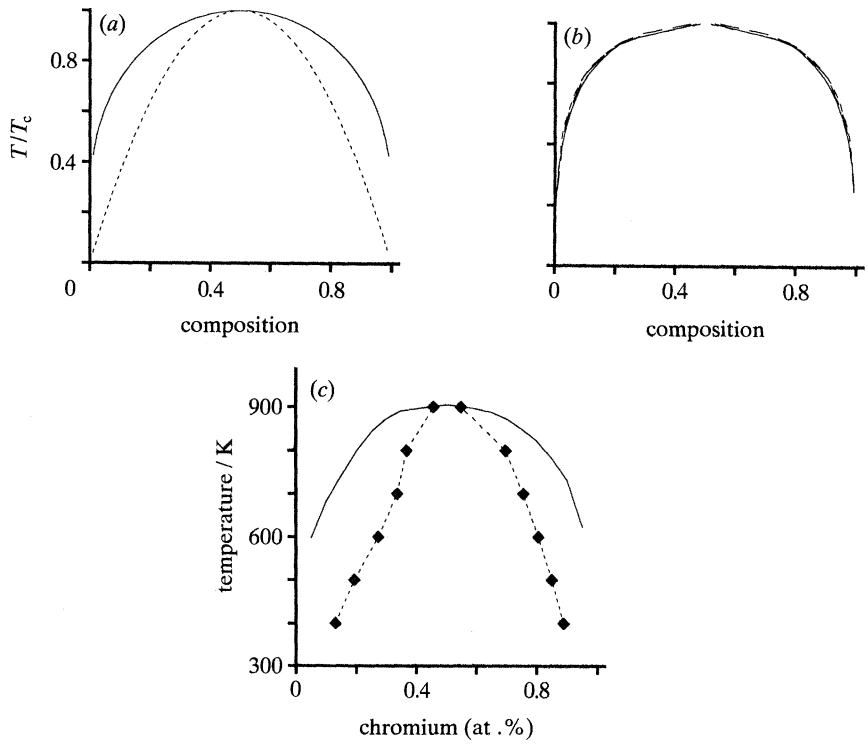

Figure 3. Phase diagrams for (*a*) the regular solution model, (*b*) the Ising model (– – –, simple cubic; ——, body centred cubic; ——, face centred cubic) and (*c*) the iron–chromium system, as calculated using the ThermoCalc thermodynamical database. In (*a*) and (*c*) the dotted line represents the spinodal region.

defines the solubility limits for the alloy, since between these compositions, the Gibbs energy can be decreased by phase separation. By finding the minima of G, the equation for the solubility limits is found to be

$$T = m\alpha(2x-1)/2k\ln[x/(1-x)].$$

PHILOSOPHICAL TRANSACTIONS OF THE ROYAL SOCIETY A MATHEMATICAL, PHYSICAL & ENGINEERING SCIENCES

Table 1. *Critical energy parameters* (α/kT_c) *expected from the mean field model, compared with those calculated from the simulation*

lattice	simple cubic	body-centred cubic	face-centred cubic
coordination number (m)	6	8	12
expected critical parameter	0.75	0.5	0.33
calculated critical parameter	0.86	0.62	0.40

The critical temperature, which is the top of the miscibility gap, can be calculated from this equation by finding the limit as the composition tends to $x = 0.5$

$$T_c = \lim_{x \to \frac{1}{2}} m \frac{\alpha(2x-1)}{2k \ln [x/(1-x)]} = \frac{m\alpha}{4k}.$$

The miscibility gap can now be re-expressed in terms of the critical temperature (figure 3*a*)

$$T/T_c = (4x-2)/\ln [x/(1-x)].$$

The solubility limits for the Ising model are found by swapping atoms between two lattices of equal numbers of atoms, both initially set to 50% composition. For low values of the energy parameter α/kT, equivalent to a high model temperature, the two lattices maintain the same composition. At lower temperatures (larger α/kT values) the compositions of the two lattices diverge, reaching equilibrium compositions which are equivalent to the minima in the Gibbs energy. The phase diagrams produced in this way for both a simple cubic lattice and a face-centred cubic lattice are shown in figure 3*b*, where temperatures are plotted as a fraction of the critical temperature for each model. Both models produce essentially the same miscibility gap, which is similar in shape to that expected from the mean field theory. There were some discrepancies, however, between the expected value of the critical energy parameter, and that calculated from the simulation, as shown in table 1. The differences are probably due to the nature of the mean field approximation in describing the nearest neighbour atomic bonding. In the simulations of phase separation, the critical energy parameter was taken to be that calculated from the Ising model, rather than the value expected from the mean field theory.

4. Spinodal decomposition

Alloys with compositions in the centre of the miscibility gap shown in figure 3 are unstable, that is to say that small random fluctuations in local composition will reduce the free energy, and so these variations will be amplified. Under these conditions, phase separation occurs by spinodal decomposition, and the region of instability, delimited by the points on the Gibbs free energy curve for which $d^2G/dx^2 = 0$, is termed the chemical spinodal. Additional energy terms, due to strain for example, are ignored in this treatment. The equation for the chemical spinodal in the mean field model is given by

$$T/T_c = 4x(1-x)$$

and this is shown in figure 3*a*. The phase diagram calculated for the iron–chromium system using the ThermoCalc thermodynamic database (figure 3*c*) shows a broad miscibility gap and a well-defined spinodal region (critical temperature $T_c = 900$ K). Iron–chromium is an ideal model system for the study of spinodal decomposition, and is also important within the context of engineering materials, for example in the

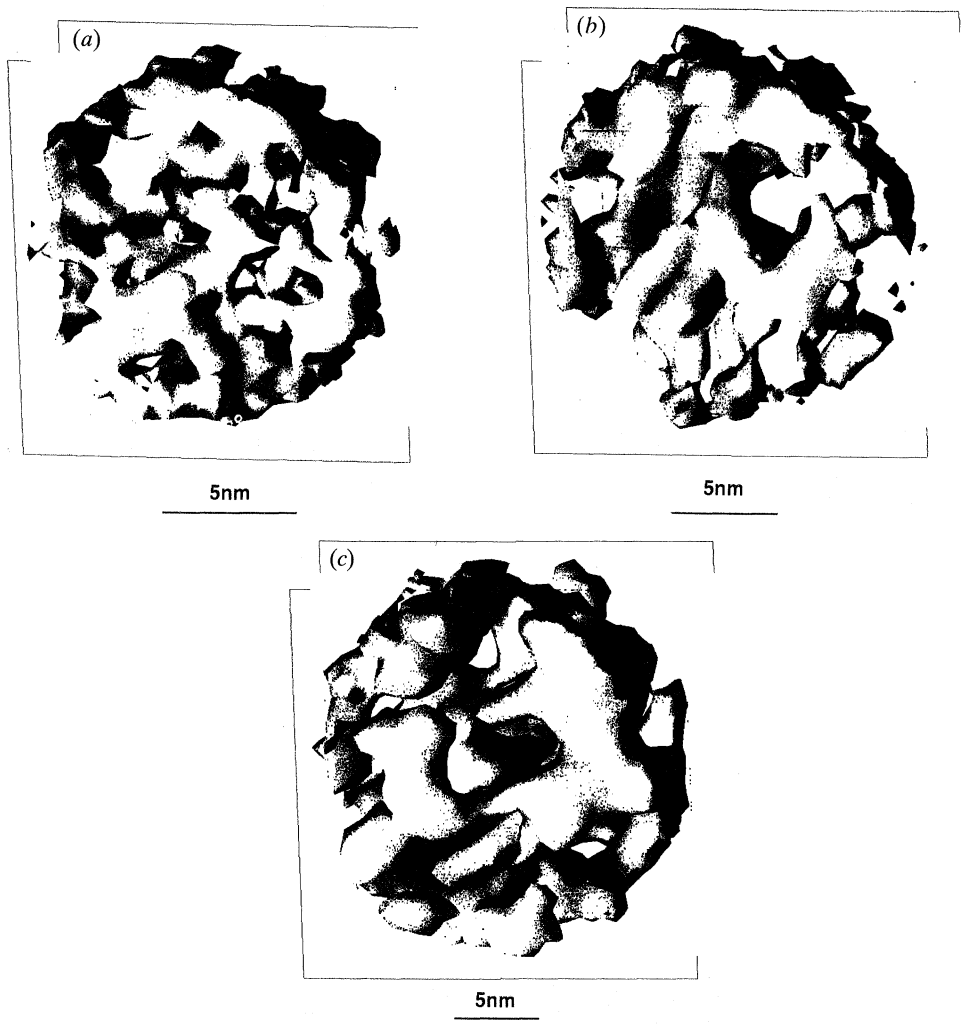

Figure 4. Isosurface reconstructions from the POSAP analysis of Fe–Cr(45 at. %) aged at 500 °C for (*a*) 24 h, (*b*) 100 h and (*c*) 500 h, showing the development in scale during ageing. Note the slight difference in scale in (*c*).

nuclear and chemical industries. The phases formed during decomposition have a small lattice mismatch (0.6%), leading to minimal coherency strain. Spinodal decomposition in this system is largely free from competing reactions: the only other phase present (σ) forms too slowly to be observed under most conditions. The present work forms part of an extensive study of the phase separation in iron–chromium by atom probe and POSAP analysis, comparing the experimental results with the Monte Carlo simulations (Hyde *et al.* 1992). A series of isosurface reconstructions from Fe–Cr(45 at. %) aged for a range of times at 773 K is shown in figure 4, and indicates how the scale of the microstructure present in this alloy develops in the early stages of phase separation. Since the miscibility gap in the iron–chromium system is not quite symmetrical, the Fe–Cr(45 at. %) alloy produces a 50% volume fraction of the chromium rich phase. At these high volume fractions, the resulting microstructure has a complex, interconnected morphology.

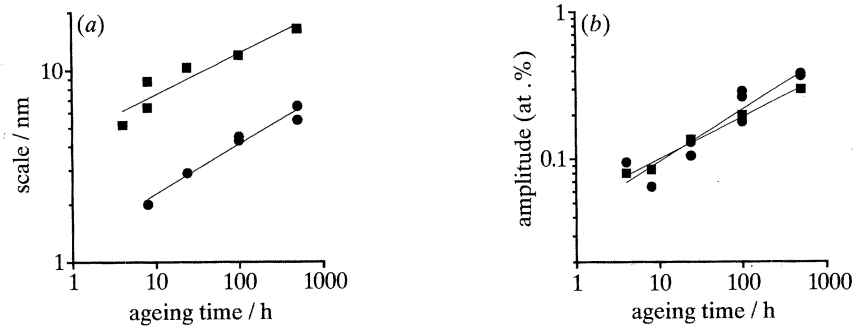

Figure 5. Kinetics of phase separation in Fe–Cr(45 at.%) aged at 500 °C as measured by conventional atom probe and position-sensitive atom probe techniques: (*a*) growth of wavelength of the microstructure; (*b*) development of composition amplitude. ●, POSAP; ■, AP.

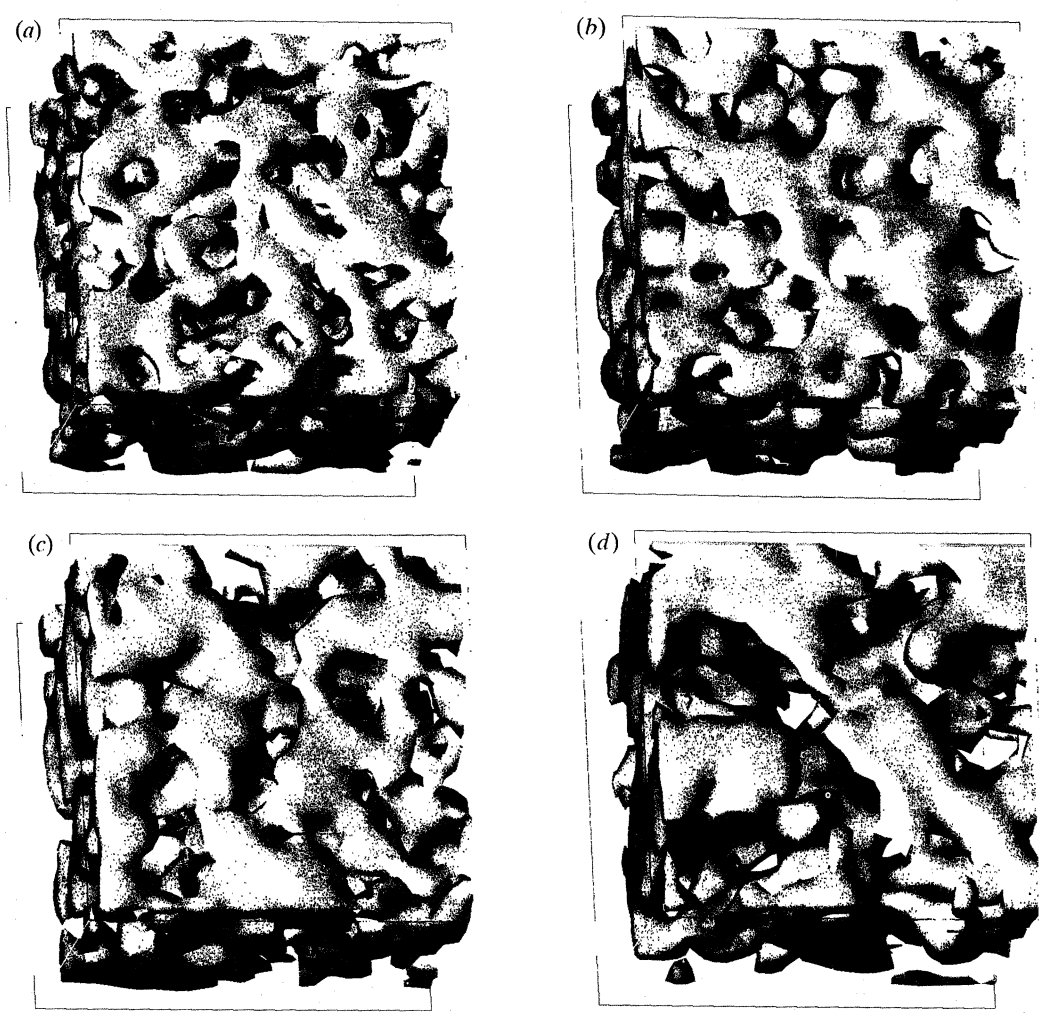

Figure 6. Isosurface representations of the microstructures in the Monte Carlo simulation of phase separation after (*a*) 10 Monte Carlo steps (MCS), (*b*) 100 MCS, (*c*) 1000 MCS, and (*d*) 10000 MCS. One MCS represents a complete sweep through the lattice, although the random selection means that given sites may be missed in any given step.

PHILOSOPHICAL TRANSACTIONS OF THE ROYAL SOCIETY A MATHEMATICAL, PHYSICAL & ENGINEERING SCIENCES

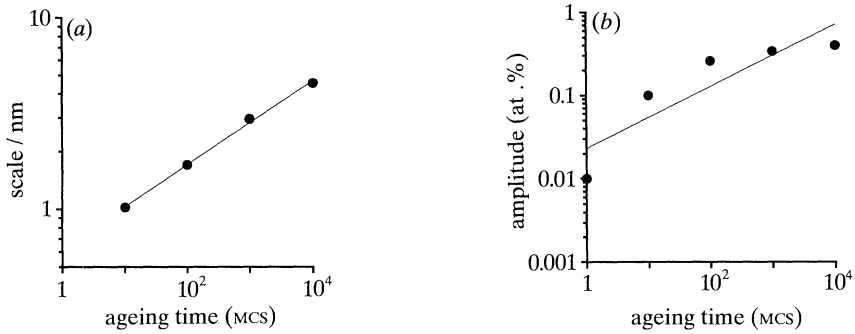

Figure 7. Kinetics of phase separation in the Monte Carlo simulation: (*a*) change in wavelength; (*b*) development of composition amplitude.

The conventional formulation of the theory of spinodal decomposition is due to Cahn & Hilliard (1958). In their model, they consider the local composition at given points in the alloy as a continuous variable, and the composition fluctuations as a series of Fourier components. The process of decomposition is treated as the selective growth of these components of composition fluctuation, and this theory predicts that in the early stages the composition amplitude grows exponentially, with a small range of wavelengths dominating. In the earliest stages, therefore, the wavelength of the microstructure should remain approximately constant. The experimentally observed growth behaviour is usually different from that predicted by this model, as shown for the case of Fe–Cr(45 at. %) in figure 5. Even from the earliest stages of phase separation accessible to the atom probe techniques, the wavelength is observed to grow (figure 5*a*). The observed growth of the structure can be fitted to a t^a power law, with a time scaling of $a = 0.21$ for the atom probe data and $a = 0.26$ for the POSAP results. There is no indication of an exponential increase in the composition amplitude (figure 5*b*), even though it was possible to determine the magnitude of the fluctuations down to below 10 at. % in structures with wavelengths of approximately 1 nm. Fitting a t^a power law once again, the measured time exponent from the atom probe is $a = 0.29$, and the POSAP results give $a = 0.36$.

An equivalent set of measurements from the Monte Carlo simulation of phase separation in the Ising model is shown in figures 6 and 7. Modelling was carried out using a 50 % atomic fraction, which yields a 50 % volume fraction of the two phases after separation, equivalent to the case of the Fe–Cr(45 at. %) alloy analysed experimentally. A modelled temperature of 800 K was established by comparing the critical energy parameter of the model with the critical temperature of the iron–chromium system calculated from the ThermoCalc database (900 K). The development of the microstructure on ageing can be seen clearly in the sequence of isosurface reconstructions shown in figure 6. By analysing the atomic positions from the model in exactly the same way as for the POSAP data, the rate of growth of the wavelength and the amplitude of composition fluctuations can be determined from the simulation (figure 7*a*, *b*). These were fitted to a t^a power law as for the experimental data, and it was found that the increase in scale followed a $t^{0.22}$ dependence. The composition fluctuations grew in amplitude with a $t^{0.36}$ dependence, although the fit in this case is not as good. In both cases the scaling behaviour is in good agreement with the experimental observations. The results shown here were calculated using a simple cubic lattice but simulations based on a more realistic body-centred cubic lattice showed few quantitative differences. Since spatial information present in the

PHILOSOPHICAL TRANSACTIONS OF THE ROYAL SOCIETY A MATHEMATICAL, PHYSICAL & ENGINEERING SCIENCES

POSAP data allows a full three-dimensional reconstruction of the atomic-scale chemistry present in the material, it is also possible to perform topological and morphological analysis of the microstructure, as discussed by Cerezo *et al.* (1991). This permits the ageing process to be characterized still further. For example, the fractal dimension of the interface between chromium-rich and iron-rich phases can be measured, and the change of dimension with ageing time explored. Hyde *et al.* used these techniques for a detailed comparison between the ageing of a number of iron–chromium alloys and the results from the Monte Carlo simulation. These authors found that the simulations were able to represent accurately the development of microstructural features.

5. Nucleation and growth

Outside of the spinodal region of the phase diagram (figure 3*a*), but still within the miscibility gap, the solid solution is metastable and may undergo phase separation by nucleation and growth. Composition fluctuations which are small in amplitude and extent are unstable and tend to decay, but once a nucleus of the second phase reaches a critical size, it is stable and can continue to grow. In the conventional model for this process, the nucleus is treated as a perfect sphere of radius r. Obviously, the nucleus cannot be a perfect sphere at this scale, and this is simply a continuum approximation of the problem. The free energy of the nucleus is considered to consist of a favourable volume term, due to the bonding of like atoms in the nucleus, and an unfavourable surface term which is sometimes called surface tension but may be viewed principally in terms of the binding between unlike atoms across the interface. Since the volume term varies as r^3 and the surface term as r^2, a potential barrier exists for the growth of the nucleus. When the top of the barrier is reached (at the critical size) it is energetically favourable for the nucleus to continue to grow. In practise the distinction between the regimes of spinodal decomposition and nucleation is blurred, since close to the spinodal limit, both the energy barrier for nucleation and the critical nucleus size will be small.

Once again, there exists a good model alloy for the study of nucleation and growth: copper–cobalt. The thermodynamics of the system are well established, and the phase diagram has a broad miscibility gap and no intermediate phases. Solid solubilities at both sides of the phase diagram are small so precipitates in these alloys should be almost pure cobalt or copper. These have the same face-centred cubic crystal structure, and the lattice mismatch is small (below 2%). A sequence of POSAP analyses of Cu–Co(1.0 at. %) aged at 723 K is shown in figure 8. In the earliest stages (10 min) the distribution of cobalt atoms appears to be random. After ageing for $\frac{1}{2}$–1 h, clusters of cobalt atoms (embryos) can be seen, and statistical analysis shows the distribution to be non-random. Ageing for 24 h produces a distribution of nuclei approximately 1.5 nm in diameter of almost pure cobalt (over 90 at. %).

Is it possible for a simple Monte Carlo simulation to adequately represent this behaviour? At first, it might seem not, since whatever the size of a nucleus, moving a cobalt atom from the matrix to the surface of the nucleus will always decrease the free energy if the mean composition is in the miscibility gap. However, the formation of a nucleus greatly reduces the entropy of the system, and although this is not considered explicitly in the simulation, the stochastic nature of the algorithm effectively incorporates entropy in the model. The behaviour of the Ising model can therefore be treated using standard gibbsian thermodynamics. Consider a system of

PHILOSOPHICAL TRANSACTIONS OF THE ROYAL SOCIETY A MATHEMATICAL, PHYSICAL & ENGINEERING SCIENCES

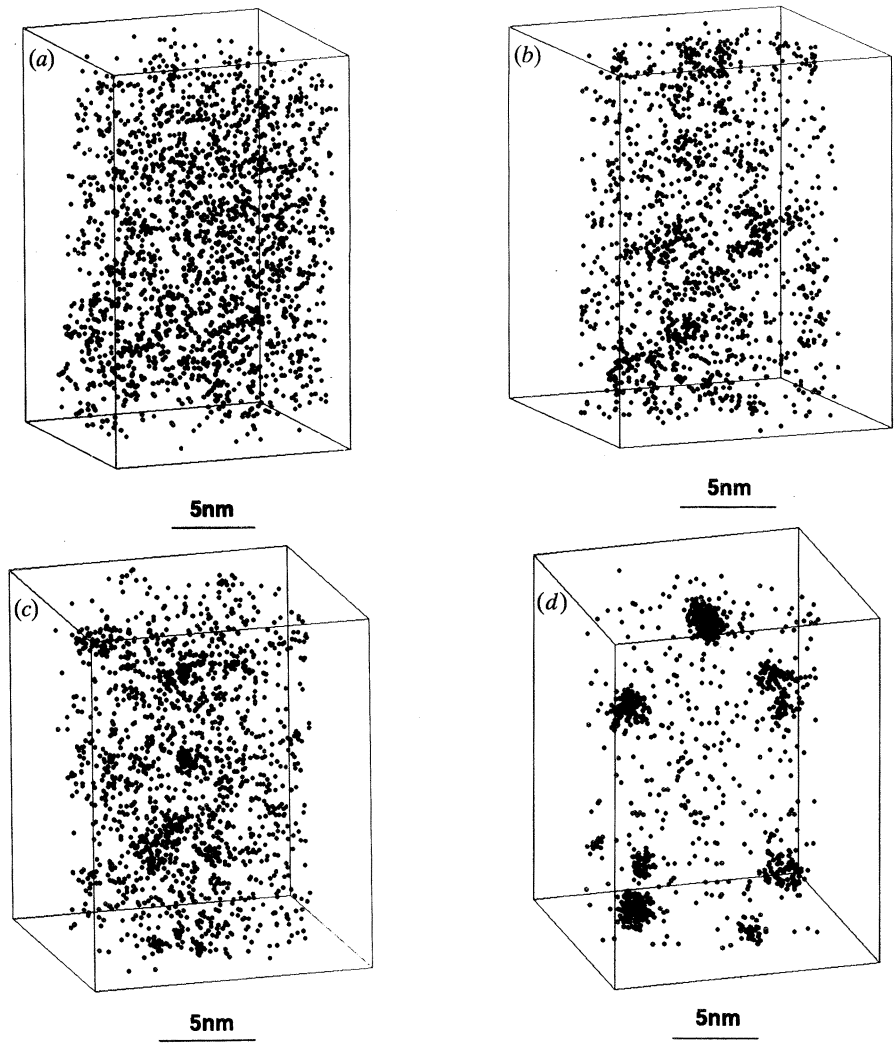

Figure 8. Distribution of cobalt atoms from the POSAP analysis of Cu–Co(1 at. %) aged at 723 K for (*a*) 10 min, (*b*) 30 min, (*c*) 2 h and (*d*) 24 h, showing the growth of cobalt precipitates.

N atoms, as before, in which a nucleus of N_c atoms of composition x_c is formed. The composition x_m of the remaining N_m matrix atoms is given by

$$N_m(x-x_m) = N_c(x_c-x).$$

The change in free energy in forming the nucleus is therefore

$$\Delta G = N_c[g(x_c)-g(x)]+N_m[g(x_m)-g(x)]+\tfrac{1}{2}N_i\, m[E_{bb}-E_{ab}]\, x_c,$$

where $g(x)$ is the Gibbs free energy per atom of a regular solution of composition x, and N_i is the number of B atoms which are at the interface of the cluster. It is assumed that on average the interface atoms have half of their bonds to the precipitate, and half to the matrix. Using the approximation of a spherical particle, the number of interface atoms can be calculated as

$$N_i = \sqrt[3]{(36\pi N_c^2)}.$$

Figure 9

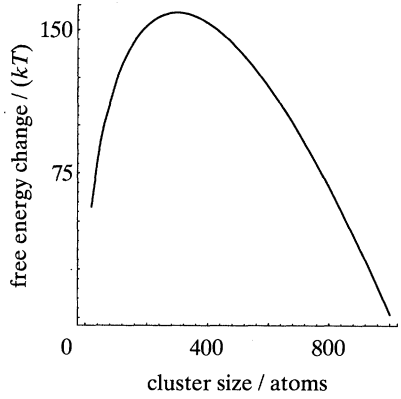

Figure 10

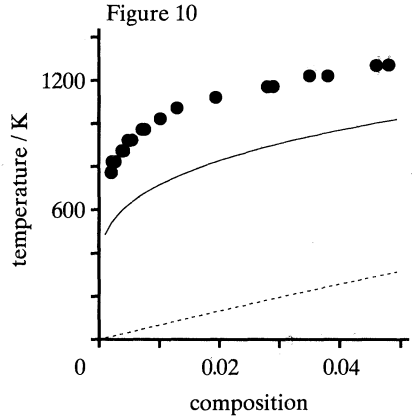

Figure 9. Variation in free energy gain between a random solid solution and a distribution of clusters as a function of the cluster size for a temperature of 0.43 T_c and a composition of 4 at. %. The energy barrier to the growth of nuclei is clearly seen, and under these conditions the critical nucleus size is just over 300 atoms.

Figure 10. Copper–cobalt phase diagram from the data compiled by Nishizawa & Ishida (1984) (●) compared with the miscibility gap (——) and chemical spinodal (· · · ·) for the Ising model, assuming a critical temperature of $T_c = 1680$ K.

In the limit of $N_m \gg N_c$, the change in the free energy of the matrix is given by

$$N_m[g(x_m)-g(x)] = N_m[x-x_m]\left[\frac{dg}{dx}\right]_{x=x_m} = N_c[x_c-x]\left[\frac{dg}{dx}\right]_{x=x_m}$$

Substituting for the critical temperature from above gives an expression for the total free energy change:

$$\Delta G = N_c\left[g(x_c)-g(x)+[x_c-x]\left[\frac{dg}{dx}\right]_{x=x_m}\right]+x_c\sqrt[3]{(36\pi N_c^2)}\,k\,T_c.$$

The variation in free energy as a function of cluster size is shown in figure 9 for a temperature of 0.43 T_c and a composition of 4 at. %, calculated assuming that the nuclei formed are of the composition which gives a minimum in the Gibbs free entry ($x \approx 1-e^{-2T_c/T}$). There is an energy barrier of approximately 170 kT to the growth of nuclei, and the critical nucleus size is below 300 atoms.

Since the copper–cobalt phase diagram does not permit the assignment of a critical temperature due to an intervening peritectic reaction, a critical temperature of 1680 K was used for the Monte Carlo simulations, based on the estimate by Chisholm (1986) who fitted a sub-regular solution model to the alloy solubility data for temperatures in the range 800–1400 K. However, the Ising model is essentially a regular solution, and the use of the critical temperature from a sub-regular model leads to a discrepancy between the phase diagrams of model and the alloy. A comparison of the miscibility gap in the Ising model, assuming a critical temperature of $T_c = 1680$ K, and some of the solubility data for copper–cobalt alloys compiled by Nishizawa and Ishida (1984) is shown in figure 10. The degree of undercooling for a given composition will be underestimated in the simulation, and the undercooling for a 1 % alloy is approximately equal to that of the simulation at a 4 % atomic fraction.

The results of a Monte Carlo simulation for a 4 % atomic fraction at a temperature of 0.43 T_c (equivalent to 723 K for $T_c = 1680$ K) are shown in figure 11. A graph of

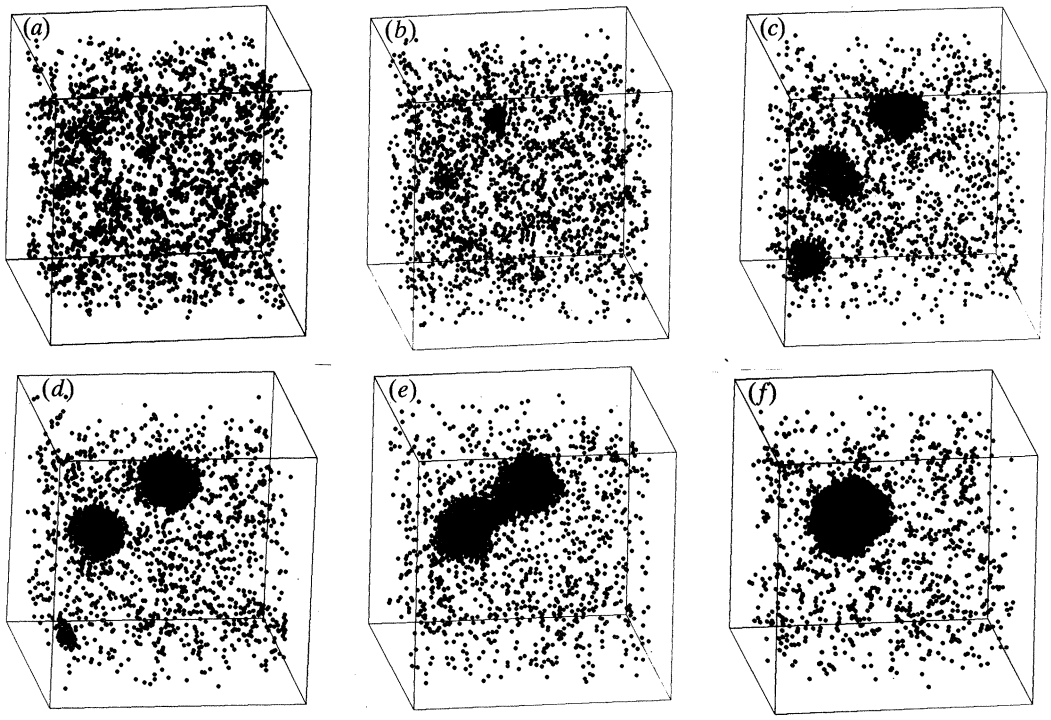

Figure 11. Atom positions from a Monte Carlo simulation of ageing in an Ising model, for an atomic fraction of 4% and a temperature of 0.43 T_c after (*a*) 2000 MCS, (*b*) 2750 MCS, (*c*) 5750 MCS, (*d*) 8500 MCS, (*e*) 14500 MCS and (*f*) 20000 MCS.

Figure 12. Graph showing the size of the largest cluster as a function of ageing time in the simulation shown in figure 10.

the size of the largest cluster as a function of ageing time in the simulation is given in figure 12. From the initial random arrangement of solute atoms, embryos quickly form (figure 10*a*). There is then a period in which none of the embryos within the modelled volume exceeds the critical size. At this point the phase separation appears static, although if it were possible to model a much larger volume of material, a slow

increase in the density of critical nuclei should be observed. Finally a nucleus is formed within the model which exceeds the critical size and this grows rapidly (figure 10*b*). Two more nuclei are formed soon after (figure 10*c*) but one of these redissolves almost immediately as the other two nuclei grow (figure 10*d*). At later stages the two remaining nuclei coalesce (figure 10*e*) to form a single cobalt-rich particle (figure 10*f*). Measurements of the composition of the nuclei from the simulation show them to be essentially 100% cobalt as soon as they are formed. The phase decomposition in the model is therefore a classical one, contrary to the conclusion drawn by Chisholm & Laughlin (1987) from simulations carried out with similar parameters. That is not to say, however, that the transformation occurs classically right up to the spinodal. It is intended to perform modelling across a range of temperatures and compositions to observe how the transformation behaviour changes progressively from classical nucleation to spinodal decomposition.

It is clear from this example of a simulated ageing, that the simple model is able to reproduce many of the features which we expect to see in the process of homogeneous nucleation and growth, but at the atomic level. The 'incubation period', nucleation barrier and Ostwald ripening all seem to be represented in the particular example shown here.

6. Conclusions

Despite the extreme simplicity of the Monte Carlo simulation described here, it appears to model quite successfully many of the features of the early stages of phase transformations which are observed experimentally using the atom probe and POSAP, covering the timescales which are typical of heat treatments or thermal ageing of alloys. In modelling of spinodal decomposition, the simulation has provided quantitative fits to the dynamics of phase separation in iron–chromium alloys, including the development of microstructural features. Initial results on the modelling of nucleation and growth appear promising, although it may be some time before the same quantitative agreement is attained. Given the success of such a basic simulation method, it is hoped that further development, for example by the use more realistic interatomic potentials, will extend the usefulness of the technique to a wider range of materials, and allow the accurate modelling of the early stages of other phase transformations, such as ordering and the conditional spinodal reaction.

A.C. is grateful to The Royal Society and Wolfson College, Oxford for support during the course of this work. J.M.H. and R.P.S. thank the Science and Engineering Research Council for financial support in the form of studentships. The studies of iron–chromium are sponsored in part by the Division of Materials Sciences, U.S. Department of Energy, under contract DE-AC05-84OR21400 with Martin Marietta Energy Systems, Inc. The authors are grateful to Dr M. F. Chisholm, Oak Ridge National Laboratory for the supply of the copper–cobalt alloys used in this work. This research is being funded by the Science and Engineering Research Council under grant no. GR/H/384845.

References

Cahn, J. W. & Hilliard, J. E. 1958 Free energy of a non-uniform system I. Interfacial free energy. *J. chem. Phys.* **28**, 258–267.

Cerezo, A., Godfrey, T. J. & Grovenor, C. R. M. 1989 Materials analysis with a position-sensitive atom probe *J. Microsc.* **154**, 215–225.

Cerezo, A., Hetherington, M. G., Hyde, J. M. & Miller, M. K. 1991 A topological approach to materials characterisation. *Scripta metall.* **25**, 1435–1440.

Chisholm, M. F. & Laughlin, D. E. 1987 Decomposition in alloys: an overview. In *Phase transformations 87* (ed. G. W. Lorimer), p. 17. London: Institute of Metals.

Hyde, J. M., Cerezo, A., Hetherington, M. G., Miller, M. K. & Smith, G. D. W. 1992 Three-dimensional characterisation of spinodally decomposed iron–chromium alloys. *Surf. Sci.* **266**, 370–377.

Metropolis, N., Rosenbluth, A. W., Teller, A. H. & Teller, E. 1953 Equation of state calculations by fast computing machines. *J. chem. Phys.* **21**, 1087–1092.

Miller, M. K. & Smith, G. D. W. 1989 *Atom probe microanalysis: principles and applications to materials science*. Pittsburgh, U.S.A.: Materials Research Society.

Müller, E. W., Panitz, J. A. & McLane, S. B. 1968 The atom-probe field ion microscope *Rev. Sci. Instrum.* **39**, 83–86.

Nishizawa, T. & Ishida, K. 1984 The Co–Cu (cobalt–copper) system. *Bull. Alloy Phase Diagrams* **5**, 161–165.

Yaldram, K. & Binder, K. 1991 Spinodal decomposition of a two-dimensional model alloy with mobile vacancies. *Acta. metall.* **39**, 707–717.

PHILOSOPHICAL TRANSACTIONS OF THE ROYAL SOCIETY A MATHEMATICAL, PHYSICAL & ENGINEERING SCIENCES

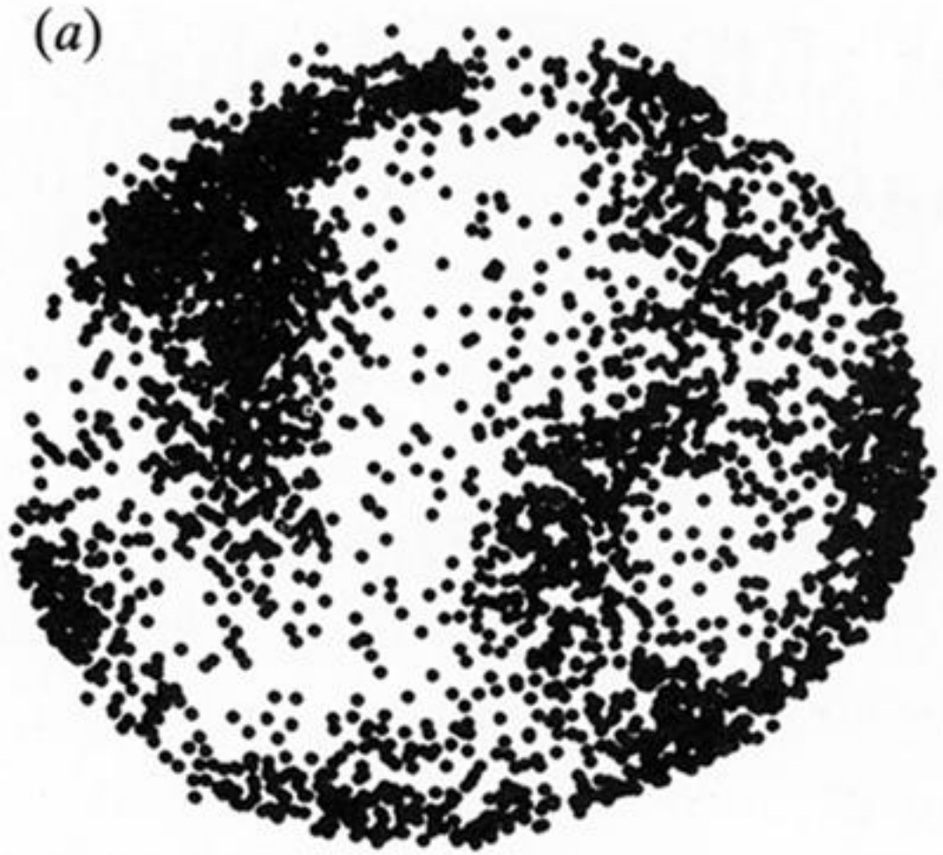

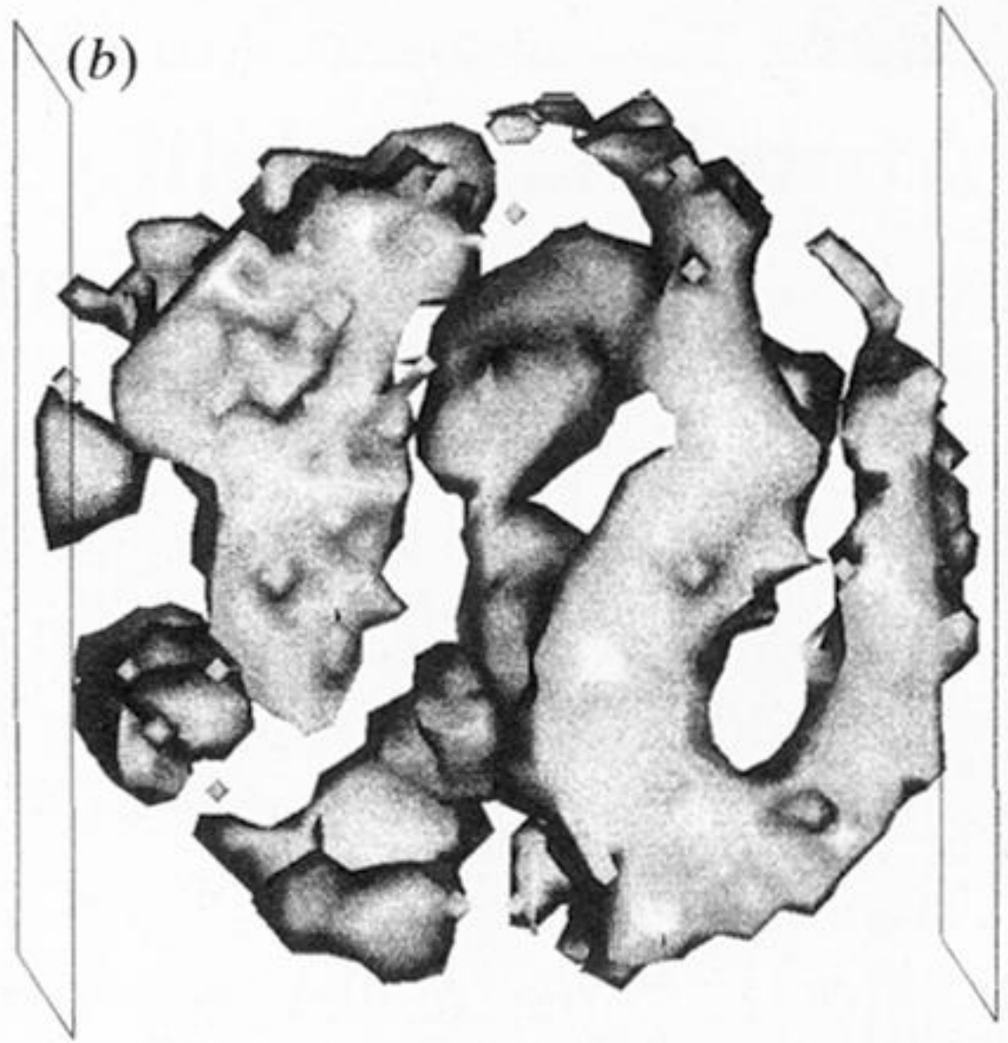

Figure 1. Position sensitive atom probe analysis of the ferrite phase in a CF3 duplex stainless steel (Fe, 21% Cr, 9% Ni, 0.4% Mn, 0.7% Si, 0.2% Mo, 0.02% C (all by mass)) aged for 10^4 hours at 400 °C. (*a*) Chromium atom map from a slice of material 2 nm deep, showing the clustering of chromium atoms into an interconnected structure during the thermal ageing. (*b*) Isosurface reconstruction of the microstructure from a region of material 15 nm in diameter and 10 nm deep. After a local sampling process, the surface is drawn through all points of composition 30 at. %, which represents the interface between chromium enriched and chromium depleted regions.

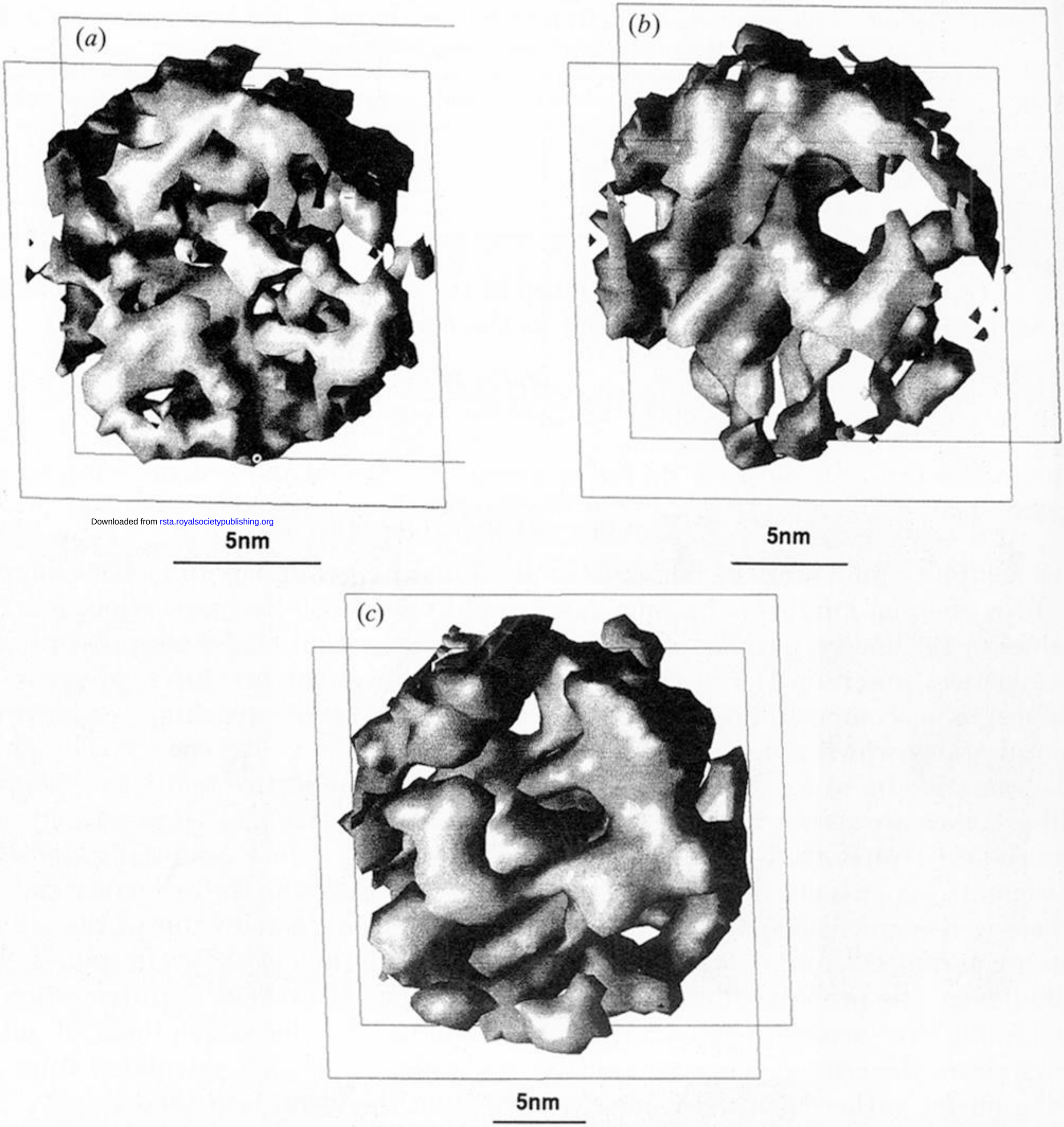

Figure 4. Isosurface reconstructions from the POSAP analysis of Fe–Cr(45 at. %) aged at 500 °C for (*a*) 24 h, (*b*) 100 h and (*c*) 500 h, showing the development in scale during ageing. Note the slight difference in scale in (*c*).

Figure 6. Isosurface representations of the microstructures in the Monte Carlo simulation of phase separation after (*a*) 10 Monte Carlo steps (MCS), (*b*) 100 MCS, (*c*) 1000 MCS, and (*d*) 10000 MCS. One MCS represents a complete sweep through the lattice, although the random selection means that given sites may be missed in any given step.